Electronic Supplementary Material (ESI) for Physical Chemistry Chemical Physics.
This journal is © the Owner Societies 2019

Supporting information of "Optimal geometry parameter for plasmonic sensitivities of individual Au nanopoarticle sensors"

ChaoLing Du,[a,]* *WanChun Yang,*[a] *Sheng Peng,*[b] *and DaNing Shi* [a]

[a]College of Science, Nanjing University of Aeronautics and Astronautics, Nanjing 211100, PR China

[b]Nanjing Univ, Natl Lab Solid State Microstruct, Nanjing 210093, PR China

*Email: cldu@nuaa.edu.cn

Supplementary Table, Figures and Text

Table 1 Parameters of the short axes of the concerned individual Au nanoparticles.

Nanoparticle	Nanodisc	Nanorod	Ellipsoid 1	Ellipsoid 2	Ellipsoid 3	Ellipsoid 4
Short axis's length in nm	5	10	10 and 10	8 and 20	8 and 40	5 and 5

Table 1 listed the length of each short axis of each the considered nanoparticles of the first set of samples in the paper, whose volume is variable and increases with the corresponding aspect ratio *AR*. To obtain *AR* for Ellipsoid 2 and 3, the corresponding square root of the short axis product is taken as their effective length of short axis, respectively.

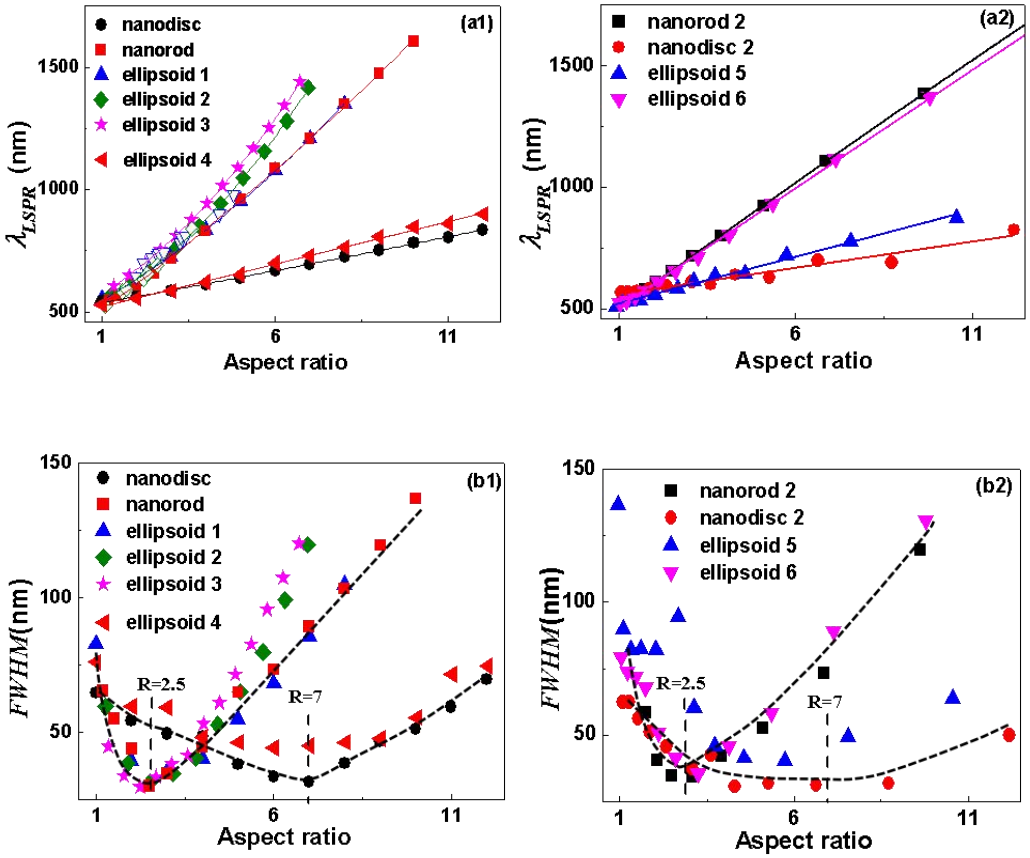

Fig. S1 The DDA calculated λ_{LSPR} (a) and corresponding *FWHM* (b) as functions of their aspect ratios, respectively, for the concerned variable (a1, b1) and invariable (a2, b2) volume Au nanoparticles. The solid lines in (a) present the fitting results while the dashed lines in (b) work as guidelines for eyes. The hollow triangles and rhombus in (a) present the experimental reported data of nanorod in Ref. [1] and [2], respectively.

Fig. S1 demonstrates that the obtained λ_{LSPR} and *FWHM* are sensitive to their *AR*, reflecting their *AR* effect. With AR increasing in Fig. S1a1 and Fig.S1b1, volume of each nanoparticles increase, hence the corresponding λ_{LSPR} and FWHM responses also reflect the size effect of each nanoparticle. The responses in Fig S1 are noted to be classified into two sets, one of prolate nanoparticles (including nanorods and prolate nanoellipsoids), and the other of oblate nanoparticles (including nanodiscs and oblate nanoellipsoids) both for variable and invariable

volume nanoparticles. Fig. S1a shows that λ_{LSPR} of the concerned prolate nanoparticles increases with *AR* quadratically while that of oblate nanoparticles increases with *AR* linearly. Fig. S1b reveals that the corresponding *FWHM* of each the concerned nanoparticles initially decreases with *AR* till gets a minimum, and then increases with *AR* increasing more regardless of nanoparticles' shapes (Fig. S1b1 and Fig. S1b2) and sizes (Fig. S1b1). An optimized *AR* for *FWHM* is unveiled for the concerned oblate nanoparticles at AR ~7.0, and for prolate nanoparticles at *AR* ~2.5, respectively. Then, we turn to Fig. S1a to check the corresponding λ_{LSPR} at these two *AR*, both of which are revealed to locate at ~700nm. This is understandable as *FWHM* of our concerned Au nanoparticles obeys the following equation [3]

$$FWHM = 2\varepsilon_i \mid_{LSPR} / \left| \frac{d\varepsilon_r}{d\lambda} \mid_{LSPR} \right| \qquad (1)$$

Here λ , ε_i , and ε_r is the incident light wavelength, the imaginary and real part of Au dielectric constant at their λ_{LSPR} , respectively. By checking Au dielectric constants in experiments [4], the variation of the derivative of ε_r with λ is negligible while ε_i exhibits minimum at ~700nm. Hence, the dielectric response of Au contributes to the minimum of *FWHM* for the presented nanoparticle sensors.

Additionally, Fig. S1 reveals that at a specific *AR*, both λ_{LSPR} and *FWHM* of nanorods, nanoellipsoids and nanodiscs are different, reflecting their shape effect. Meanwhile, the small difference between λ_{LSPR} of the three nanoellipsoids 1, 2 and 3 owns to the differences of their size perpendicular to the incident polarization, which effect is shown to be less obvious than that of shapes and aspect ratios.

Fig. S2(a) and Fig. S2(b) give the typical electric-field $|E|$ distributions of the *y-z* cross-sections around the concerned nanoparticles with aspect ratio 3.0 and 8.0, respectively. The obtained different $|E|$ distributions reflects their *AR* effect, hence size effect while the different $|E|$ distributions at the same *AR* reflect their different shape effect. These further lead to their different extinction spectra, hence λ_{LSPR} and *FWHM* as presented in Fig. S1.

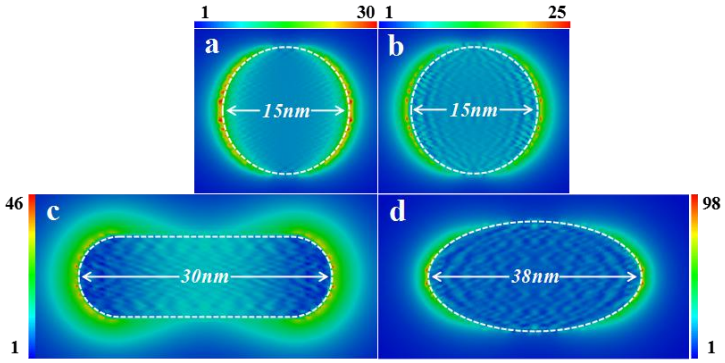

Fig. S2(a) Typical electric-field $|E|$ distributions of the *y-z* cross-sections around the concerned nanodisc (a), oblate nanoellipsoid (b), nanorod (c), and prolate nanoellipsoid (d) with each of the aspect ratio being 3.0.

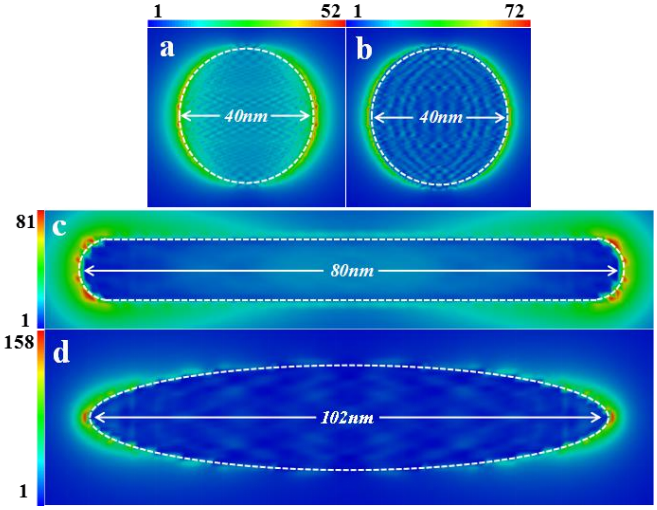

Fig. S2(b) Typical electric-field $|E|$ distributions of the *y-z* cross-sections around the concerned nanodisc (a), oblate nanoellipsoid (b), nanorod (c), and prolate nanoellipsoid (d) with each of the aspect ratio being 8.0.

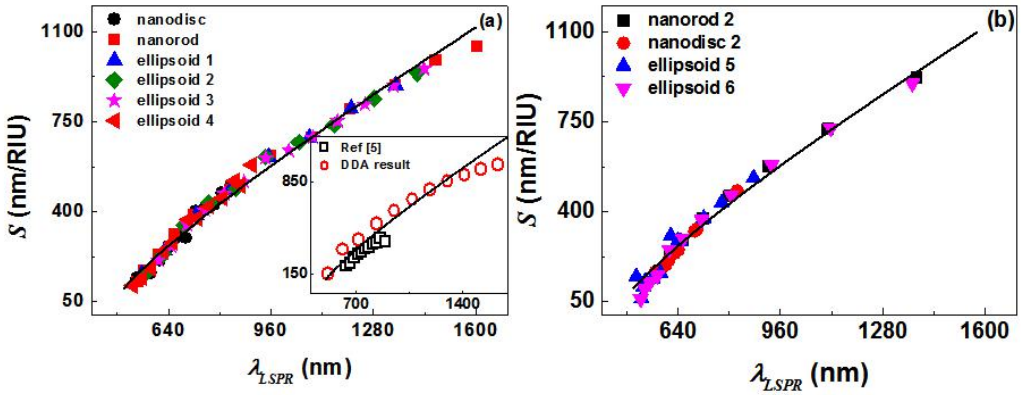

Fig. S3 The DDA calculated *S* as a function of the corresponding λ_{LSPR} for the concerned variable (a) and invariable (b) volume Au nanoparticles. The solid lines present the nonlinear fitting results. The hollow triangles and rhombus in (a) present the available experimental reported data of nanorod in Ref. [1] and [2], respectively. The solid line of the inset of (a) presents the prediction results by the sensitivity equation in Ref.[5].

To better mimic experimental reports in Ref. [5], DDA calculation is performed for Au nanorods with the same width 20nm but different *AR*. The obtained variation of the corresponding *S* with λ_{LSPR} is plotted as the inset of Fig. S3a, which shows only a little larger value than experiments owing to the substrate effect introduced therein. It is also noted to agree well with the predictions by sensitivity equation of $S(\lambda) = \frac{\lambda}{n}(1 - \frac{\lambda_p^2}{\lambda^2} n_\infty^2)$ therein [5].

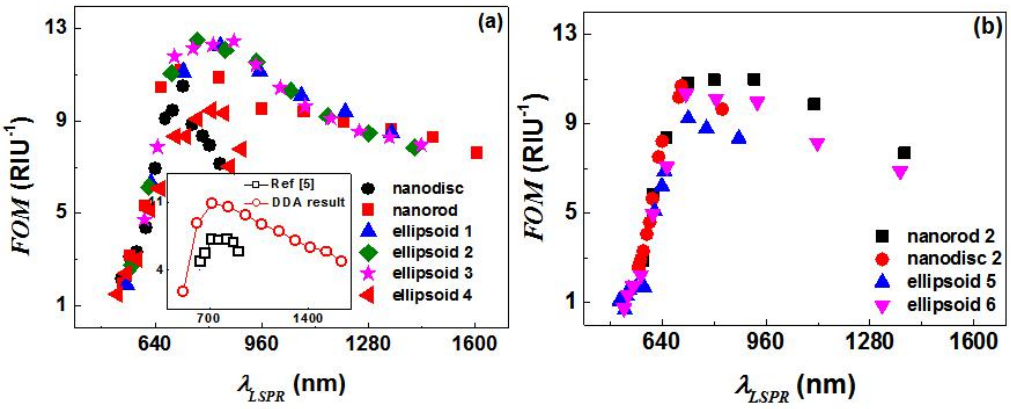

Fig. S4 The DDA calculated *FOM* as a function of the corresponding λ_{LSPR} for the concerned variable (a) and invariable (b) volume Au nanoparticles. The inset of (a) presents the comparison between DDA calculation and that of experiment data in [5] under the same geometry parameter setting for nanorod with width being 20nm. DDA calculation is shown to overestimate that of experiments, which may come from the substrate effect introduced therein [5].

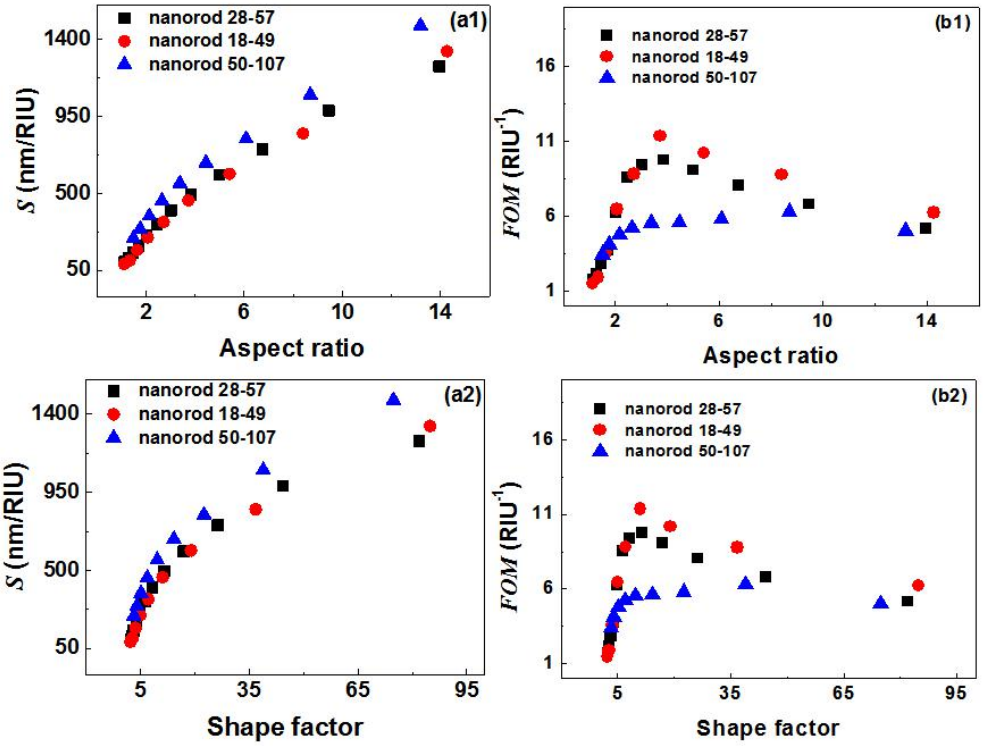

Fig. S5 The DDA calculated *S* and *FOM* as functions of *AR* (a1, b1) and shape factor (a2, b2) for Au nanorods. Rods herein are set to be the same with that of single experiments available nanorods [5] with width/length being 28/57nm, 18/49nm, and 57/107 nm, respectively.

References in the supporting information

[1] Perez JJ, Rodriguez GB, Mulvaney P. Optical control and patterning of gold-nanorod-poly(vinyl alcohol) nanocomposite films. Adv. Funct. Mater. 15 (2005) 1065-1071.

[2] Zheng YD, Xiao MD, Jiang SX. Coating fabrics with gold nanorods for colouring, UV-protection, and antibacterial functions. Nanoscale. 5 (2013) 788-795.

[3] Huang WC, Lue JT. Quantum size effect on the optical properties of small metallic particles. Phys. Rev. B. 49 (1994) 17279-17285.

[4] Johnson PB, and Christy RW. Optical constants of noble metals. Phys. Rev. B. 6 (1972) 4370-4739.

[5] Arpad J, Christina R, Yuriy K, Jan B, Andreas T, Ulrich H, and Carsten S. Highly sensitive plasmonic silver nanorods. Acs Nano. 5 (2011) 6880-6885.